Journal of Power Sources 246 (2014) 417–422

Contents lists available at ScienceDirect

Journal of Power Sources

journal homepage: www.elsevier.com/locate/jpowsour

Oxalic acid-assisted combustion synthesized $LiVO_3$ cathode material for lithium ion batteries

X.M. Jian [a], H.Q. Wenren [b], S. Huang [a], S.J. Shi [a], X.L. Wang [a], C.D. Gu [a], J.P. Tu [a,*]

[a] State Key Laboratory of Silicon Materials, Key Laboratory of Advanced Materials and Applications for Batteries of Zhejiang Province and Department of Materials Science and Engineering, Zhejiang University, Hangzhou 310027, China
[b] Zhejiang GBS Energy Co., Ltd., Ningbo 315400, China

HIGHLIGHTS

- We synthesize $LiVO_3$ by a simple combustion method followed by calcinations.
- Oxalic acid plays a role of fuel in the synthesis process.
- It also can promote the mixture of the reactants.
- $LiVO_3$ calcined at 450 °C for 2 h displays optimal electrochemical performances.
- Chemical diffusion coefficient of Li-ion is calculated by EIS and GITT.

ARTICLE INFO

Article history:
Received 5 April 2013
Received in revised form
19 July 2013
Accepted 29 July 2013
Available online 6 August 2013

Keywords:
Lithium metavanadate
Chemical diffusion coefficient
Cathode
Lithium ion battery

ABSTRACT

$LiVO_3$ materials are synthesized by combustion method with oxalic acid as fuel. Owing to its relatively low crystallization and small particle size, the $LiVO_3$ calcined at 450 °C for 2 h displays optimal electrochemical performances, delivering a high discharge capacity of 298.4 mAh g^{-1} and 262.5 mAh g^{-1} between 1.0 and 3.5 V at a current density of 50 mA g^{-1} and 500 mA g^{-1} respectively, and exhibiting good cyclic stability. In this work, the chemical diffusion coefficient of Li^+ (D_{Li+}) in the $LiVO_3$ electrode is determined by electrochemical impedance spectroscopy (EIS) and galvanostatic intermittent titration technique (GITT). The value calculated by EIS is in the range of 10^{-9}–10^{-8} cm^2 s^{-1}, while it calculated by GITT is $10^{-9.5}$–10^{-8} cm^2 s^{-1}.

1. Introduction

Lithium ion batteries (LIBs) are used in large scale for their high energy density, low self-discharge and long cyclic life. They are important for consumer electronic devices, portable power tools and vehicle electrification [1–3]. There are a lot of researches which aim at seeking for excellent cathode materials to satisfy the demand of the better battery performance. One of promising candidates is the vanadium oxides and vanadium derivatives for vanadium possess multiple valences and there are abundant resources of vanadium [4–10]. $LiVO_3$ compound, which has been proposed by V. Pralong et al. firstly [11], is highly attractive for easy synthesis and a high specific capacity.

It is well understood that the synthetic routes will strongly influence the electrochemical performance of cathode materials [12,13]. Combustion synthesis, which is employed in the field of propellants and explosives, involves an exothermic and self-sustaining chemical reaction between the metal salts and suitable organic fuel [14]. It has an advantage of time and energy saving, and requires simple equipment and cheap reagents [15]. The method has been successfully used in the synthesis of many electrode materials for LIBs, such as $LiNi_{1/3}Mn_{1/3}Co_{1/3}O_2$ [16,17], $LiMn_2O_4$ [18], $LiFePO_4$ [19], LiV_3O_8 [20], and $ZnCo_2O_4$ [21], $Li_4Ti_5O_{12}$ [22], Co_3O_4 [23]. Combustion method is based on the reaction between inorganic reagents (generally nitrates) and organic fuels [24]. The properties of the electrode materials are also influenced by the type of the fuel [25]. Recently, many organic fuels have been used in the combustion reaction, such as urea [18,20], sucrose [26,27], starch [28], citric acid [29], glycine [17] and ethanol [30,31].

* Corresponding author. Tel.: +86 571 87952856; fax: +86 571 87952573.
E-mail addresses: tujp@zju.edu.cn, tujplab@zju.edu.cn (J.P. Tu).

0378-7753/$ – see front matter © 2013 Elsevier B.V. All rights reserved.
http://dx.doi.org/10.1016/j.jpowsour.2013.07.110

In this present work, the $LiVO_3$ compounds were synthesized by a simple combustion method followed by calcination. Herein, oxalic acid not only plays a role of fuel, but also can promote the mixture of the reactants. The effect of oxalic acid on promoting mixture of the reactants to gain a better performance of the materials had been proved in many other research works [32–34]. The structure and electrochemical properties of the $LiVO_3$ compounds synthesized for different calcination times were investigated. The chemical diffusion coefficient of Li^+ (D_{Li+}) in the electrode material was calculated by electrochemical impedance spectroscopy (EIS) and galvanostatic intermittent titration technique (GITT).

2. Experimental

The $LiVO_3$ materials were synthesized by a combustion method. $LiNO_3$ and NH_4VO_3 were used as raw materials, and oxalic acid was used as fuel. Stoichiometric $LiNO_3$ and NH_4VO_3, oxalic acid (mole ratio with the metal ions was 1:1) were grounded using mortar and pestle for 1 h. At the impact of oxalic acid, those raw materials would become brown slurry. Then the slurry was put into a crucible and dried in an oven at 90 °C. At last the crucible was put into a muffle furnace which was preheated to 450 °C and calcined at this temperature for a few hours. In this work, four samples were studied with calcination for 1 h, 2 h, 3 h and 4 h to understand the effect of calcination time. The as-synthesized compounds were named as CS-1h, CS-2h, CS-3h and CS-4h for short. The morphologies and structures of the powders were characterized by scanning election microscopy (SEM, HITACHI SU70) and X-ray diffraction (XRD, Philips PC-APD with Cu Kα radiation).

The working electrode was prepared by a slurry coating procedure. The slurry consisted of 80 wt.% $LiVO_3$ powder, 10 wt.% carbon conductive agent and 10 wt.% polyvinylidene fluoride (PVDF) as a binder was coated on aluminum foil. After drying in an oven at 90 °C for 24 h, the sample was pressed under a pressure of 10 MPa. A metallic lithium foil was used as anode, 1 M $LiPF_6$ in ethylene carbonate (EC)–diethyl carbonate (DEC) (1:1 in volume) as the electrolyte and polypropylene microporous film (cellgard 2300) as separator. The CR2025 coin-type cells were assembled inside a glove box full of high-purity argon. The galvanostatic charge–discharge tests were conducted on LAND battery program control test system (Wuhan, China) between 1.0 V and 3.5 V at current densities of 50 and 500 mA g^{-1}. The cells were charged and discharged at the same current density. EIS measurements were performed on CHI604B electrochemical workstation using a three-electrode cell with the metallic lithium foil as both the reference and counter electrodes at discharge state. The amplitude of the AC signal was 5 mV over a frequency range from 100 kHz to 10 mHz. For GITT measurement, the LAND battery test system was programmed to supply a constant current flux (20 mA g^{-1}) for a given period (10 min) followed by an open-circuit stand of the cell for a specified time (40 min). This procedure was repeated for the full potential window of 1.0–3.5 V (vs. Li/Li^+).

3. Results and discussion

The XRD patterns of the compounds prepared at different calcination periods are shown in Fig. 1. All the patterns are almost similar, and the diffraction peaks can be indexed to the $LiVO_3$ phase (JCPDS card No. 70-1545) with C2/c space group, except the pattern of CS-1h. The weak peak of impurity in CS-1h, which has been marked in the figure by a flower marker, indicates that the reaction is not complete due to too short calcination time. The impurity will affect the electrochemical performance of the compound. With the increase of the calcination time, the peak intensity of $LiVO_3$ becomes strong, indicating high crystallization

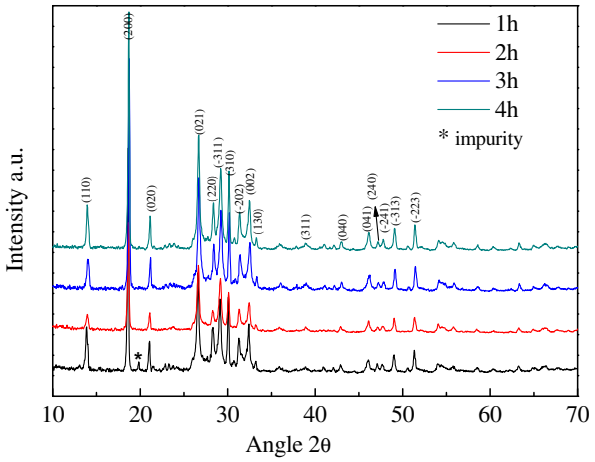

Fig. 1. XRD patterns of $LiVO_3$: (a) CS-1h; (b) CS-2h; (c) CS-3h; (d) CS-4h.

of the compound. It is known that the diffusion paths of Li^+ in the materials with higher crystallization become longer which is disadvantage for the electrochemical properties [35,36]. So it can be expected that the compound with short calcination time will exhibit good electrochemical performance. Fig. 2 shows the SEM images of $LiVO_3$ powders. CS-2h is composed of small particles, while the others are composed of agglomerated particles. The agglomerated morphology of CS-1h may be the incomplete reaction for the limitation of calcination time. When the calcination times become longer as in CS-3h and CS-4h, the particles tend to grow and agglomerate with each other. From the XRD and SEM analysis, we expect that CS-2h will have a better electrochemical performance.

Fig. 3a and c shows the initial charge–discharge curves of the $LiVO_3$ electrodes between 1.0 and 3.5 V at a current density of 50 mA g^{-1} and 500 mA g^{-1}, respectively. It is noted that the shapes of the initial charge–discharge curves are almost the same. CS-2h delivers an initial capacity of 298.4 mAh g^{-1} at a current density of 50 mAh g^{-1}, higher than CS-1h (277.2 mAh g^{-1}), CS-3h (286.4 mAh g^{-1}) and CS-2h (283.4 mAh g^{-1}). At a high current density of 500 mA g^{-1}, CS-2h still delivers the highest initial discharge capacity among the electrodes. The cyclic performance of the $LiVO_3$ electrodes is displayed in Fig. 3b and d. After 100 cycles, CS-2h can still sustain a discharge capacity of 140.8 mAh g^{-1} at a current density of 500 mA g^{-1}, showing good capacity retention at a relatively high current density. Because of the impurity existence or the agglomerated morphology, CS-1h, CS-3h and CS-4h show poor cyclic performance compared with CS-2h. Fig. 4 shows the rate capability of CS-2h between 1.0 and 3.5 V. At a low current density of 50 mA g^{-1}, the electrode delivers a high discharge capacity of 295.9 mAh g^{-1}. Even at a high current density of 800 mA g^{-1}, it can still deliver a discharge capacity of 160.5 mAh g^{-1}. When the current density is returned to 50 mA g^{-1}, the discharge capacity can be recovered to 258.6 mAh g^{-1}, revealing good electrochemical reversibility.

Fig. 5 shows the Nyquist plots of the $LiVO_3$ compounds prepared for different calcination periods. All the Nyquist plots are consisted of three parts. The first one is an intercept at Z′ axis in high frequency and the second is a depressed semicircle in the middle frequency region, while the last is the Warburg-type element (the sloping line) in the low frequency region. An intercept at Z′ axis in high frequency corresponds to the ohmic resistance of electrode. The depressed semicircle in the middle frequency range is assigned to the charge transfer resistance and the double layer capacitance.

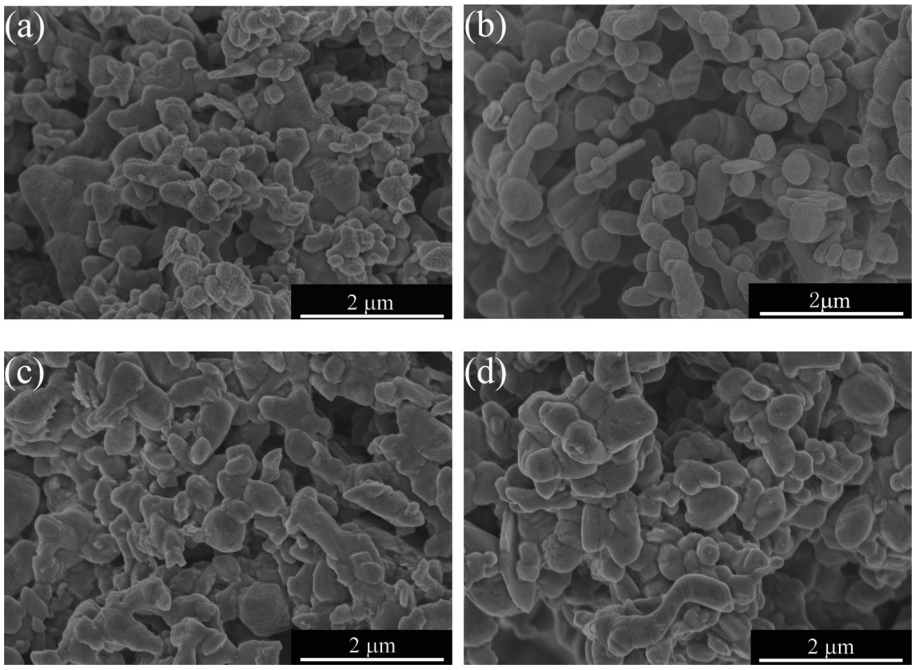

Fig. 2. SEM images of $LiVO_3$: (a) CS-1h; (b) CS-2h; (c) CS-3h; (d) CS-4h.

The low frequency Warburg impedance is related mainly to the diffusion of Li^+ in the bulk electrode [37–40]. The impedance spectra are fitted using the equivalent circuit model, as shown in Fig. 6. The fitting data are depicted in Fig. 5 by the bright green lines. A good agreement between the experimental data and fitting data obtained from the equivalent circuit is observed. The fitting parameters are summarized in Table 1. R_e represents the resistance of the electrolyte and electrode. C_f and R_f represent the resistance and capacitance of solid electrolyte interface (SEI) films, respectively. Q is associated with the capacitance of the double layer. W is Warburg impedance which is associated with the Li^+ diffusion process in the cathode materials. R_{ct} represents the charge transfer resistance of electrochemical reaction [41–44]. The smaller the resistance of the materials, the higher the electronic conductivity

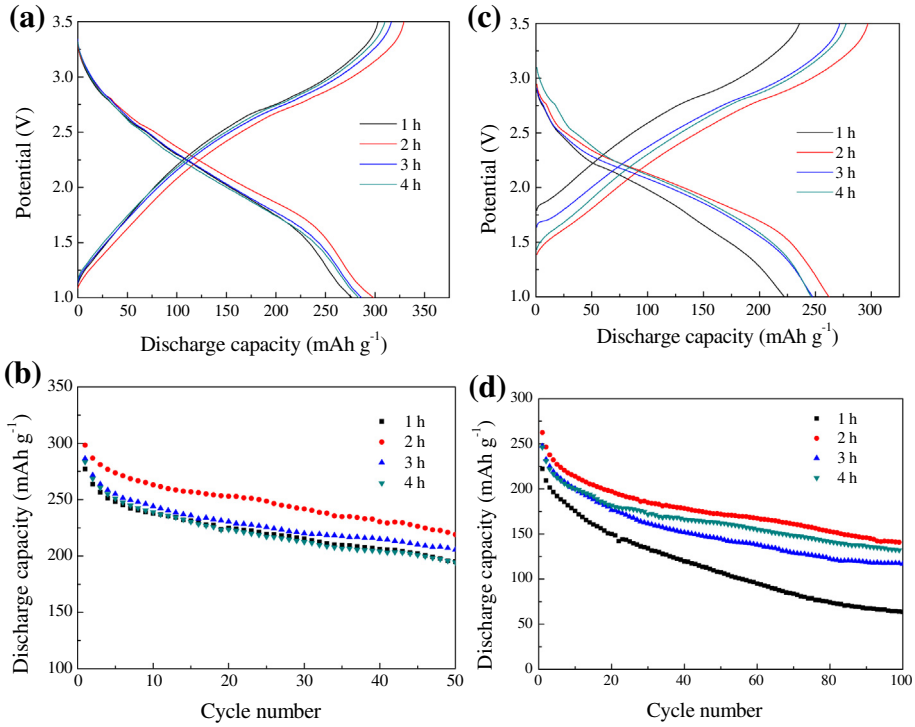

Fig. 3. (a) (b) Initial charge–discharge curves and cyclic performance at a current density of 50 mA g^{-1}, (c) (d) initial charge–discharge curves and cyclic performance at a current density of 500 mA g^{-1}.

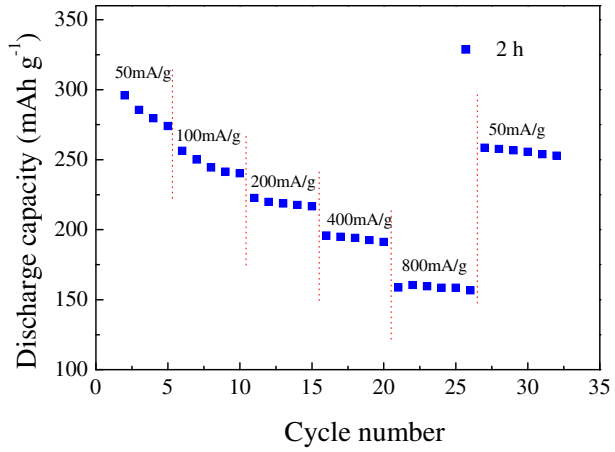

Fig. 4. Rate capacity of CS-2h at various charge–discharge current densities.

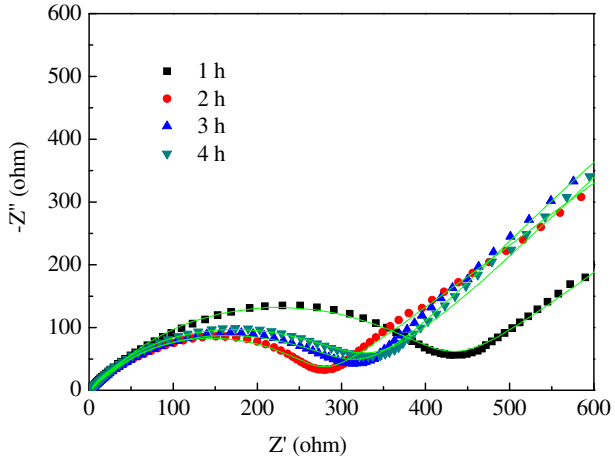

Fig. 5. Nyquist plots of $LiVO_3$ calcined for different periods after the fifth discharge.

will be. Compare the fitting parameters in Table 1, CS-2h possesses the lowest resistance R ($R = R_e + R_f + R_{ct}$), which is in accordance with the electrochemical performance presented above. As a result, the good electrochemical performance of CS-2h can be attributed to its relatively low crystallization and well particle morphology. It is known that the diffusion paths of Li^+ in the materials with higher crystallization become longer which is disadvantage for the electrochemical properties. In this work, we use EIS and GITT to calculate the chemical diffusion coefficient of Li^+ (D_{Li+}) in CS-2h.

EIS can be used to calculate the D_{Li+} in the electrode that has the low frequency Warburg impedance. Fig. 7 shows three-dimensional Nyquist plots for CS-2h. The EIS were recorded at room temperature for the first charge–discharge process at different potential. According to the model proposed by Ho et al.

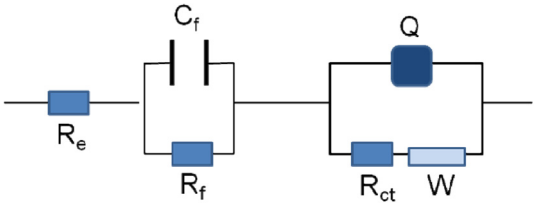

Fig. 6. The equivalent circuit model for the $LiVO_3$ electrode.

Table 1
Fitting parameters obtained from the equivalent circuit for Nyquist plots of Fig. 5.

	R_e (Ω)	R_f (Ω)	R_{ct} (Ω)	R (Ω) ($R = R_e + R_f + R_{ct}$)
CS-1h	2.524	12.22	405.9	420.64
CS-2h	3.066	7.113	262.1	272.28
CS-3h	1.930	38.03	313.4	353.36
CS-4h	2.427	396.3	322.5	721.23

[45], the D_{Li+} of Li^+ in the $LiVO_3$ compound can be calculated in the following equation:

$$D_{Li} = \frac{1}{2}\left[\left(\frac{V_M}{AF\sigma_W}\right)\frac{\delta E}{\delta x}\right]^2 \quad (1)$$

where V_M is the molar volume of the compound; A is the interface between the active material and electrolyte; F is Faraday constant (96,486 C mol^{-1}); σ_W is the Warburg coefficient. The σ_W values at different voltages are obtained from the slope of $-Z''$ vs. $\omega^{-1/2}$ plots (ω is the angular frequency) in the Warburg region (as shown in Fig. 8a and b). $\delta E/\delta x$ is the slope of the open-circuit voltage versus mobile Li^+ concentration x, which can be determined from the galvanostatic charge–discharge curve (as shown in Fig. 8c). It is obvious that Eq. (1)

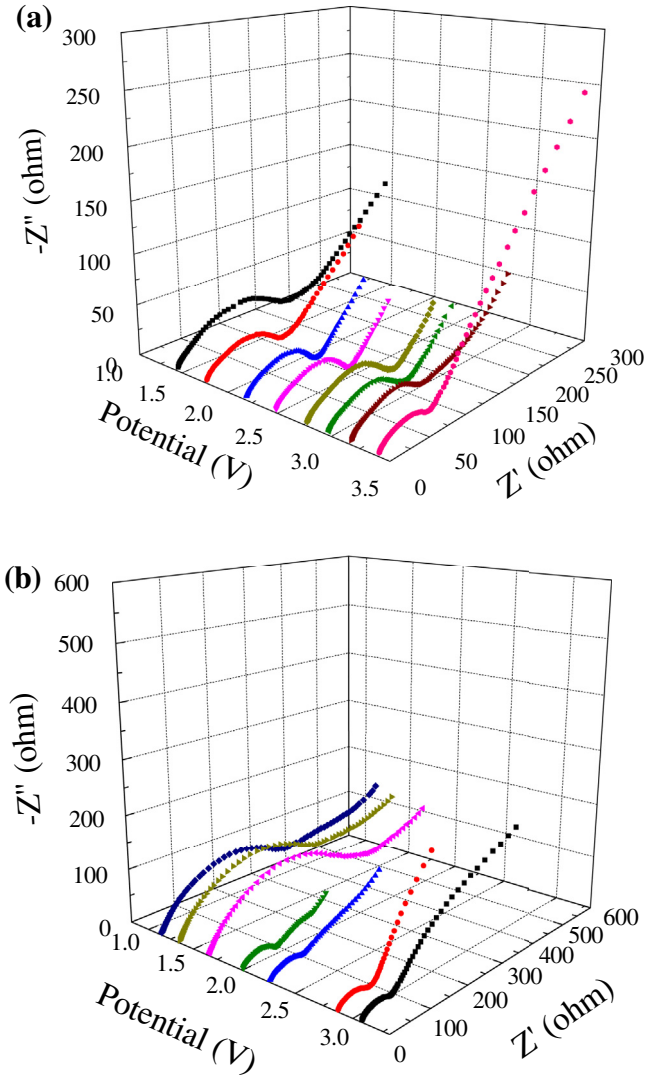

Fig. 7. Three-dimensional Nyquist plots measured at different potential for CS-2h.

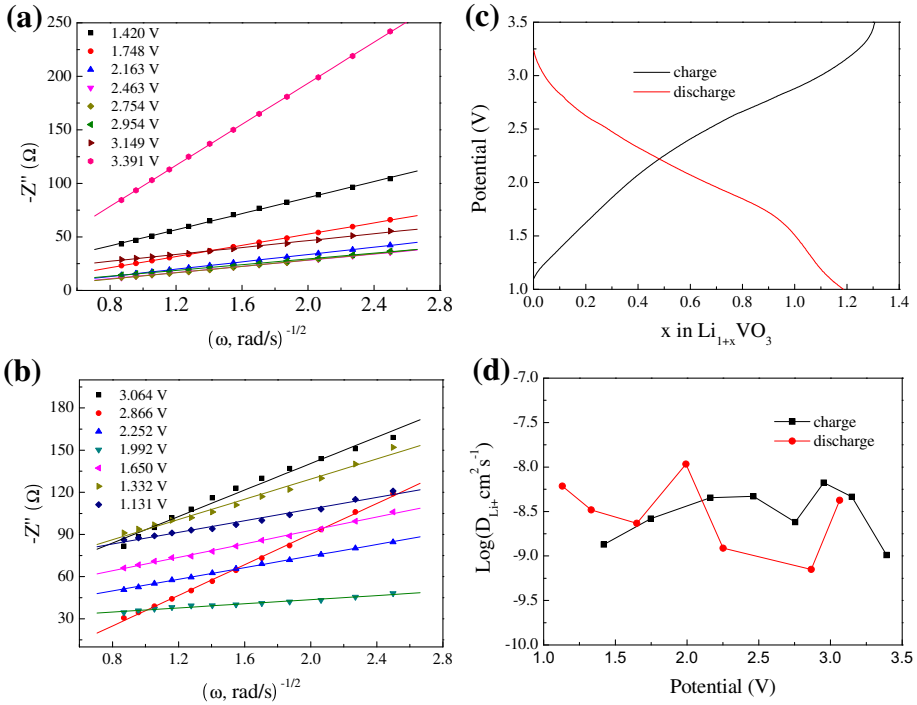

Fig. 8. The plots of the imaginary part of impedance as a function of the inverse square root of angular frequency at different voltages in the Warburg region: (a) for the first charge process (b) for the first discharge process of CS-2h; (c) the electrochemical voltage-composition curve for the $LiVO_3$ in the potential range of 1.0–3.5 V (vs. Li/Li^+) during the first galvanostatic process; (d) the calculated D_{Li+} from the EIS data for the $LiVO_3$ electrode as a function of potential during charge and discharge processes.

is suitable for the case of $LiVO_3$ because the charge–discharge curve of the electrode has no obvious plateau, which makes $\delta E/\delta x$ will never equal to zero. As shown in Fig. 8d, the calculated D_{Li+} in the $LiVO_3$ electrode is in the range of 10^{-9}–10^{-8} cm^2 s^{-1}.

GITT is considered to be a reliable method to calculate the D_{Li+} in electrodes, which has been widely applied [46–49]. Fig. 9a shows the GITT curves of CS-2h during the first cycle as a function of time in the voltage range of 1.0–3.5 V. The cell was first charged at a

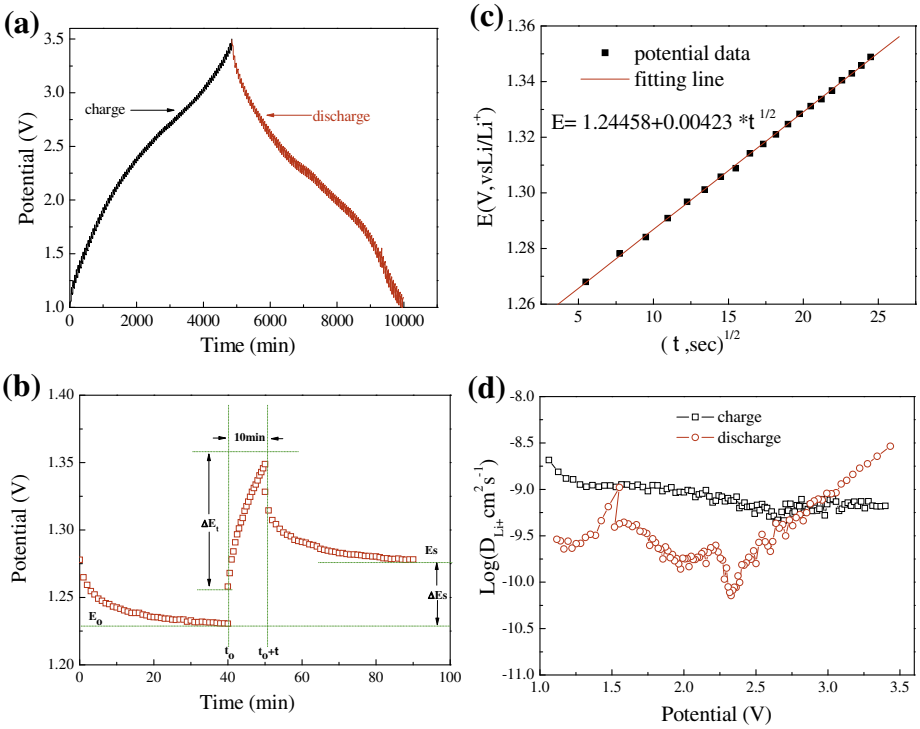

Fig. 9. (a) GITT curves of CS-2h during the first cycle as a function of time in the potential range of 1.0–3.5 V; (b) *t* vs. *E* profile of $LiVO_3$ electrode for a single GITT titration at the charge state of 1.23 V; (c) plot of voltage against $\tau^{1/2}$ to show the linear fit; (d) the calculated D_{Li+} from the GITT data for the $LiVO_3$ electrode as a function of potential during charge and discharge processes.

consent current flux (I_0 = 20 mA g^{-1}) for an interval of 10 min followed by an open-circuit stand for 40 min to allow the cell voltage to relax to its steady-state value (E_s). The applied current flux and the resulting potential profile for a single titration at the first charge state of 1.23 V is shown in Fig. 9b, with schematic labeling of different parameters, ΔE_τ, ΔE_s, etc. The D_{Li+} in the $LiVO_3$ electrode can be determined by solving Fick's second law of diffusion. Under a series of assumptions and simplifications, the D_{Li+} can be calculated by the following equation [50]:

$$D_{Li} = \frac{4}{\pi}\left(\frac{m_B V_M}{M_B A}\right)^2 \left(\frac{\Delta E_s}{\tau\left(\frac{dE_\tau}{d\sqrt{\tau}}\right)}\right)^2 \quad \left(\tau << L^2/D_{Li}\right) \tag{2}$$

where M_B is the molecular weight of the compound; V_M is the molar volume of the compound; A is the interface between the active material and electrolyte; m_B and L is the mass and the thickness of the electrode, respectively.

If E versus $\tau^{1/2}$ shows a straight line behavior during titration, Eq. (2) can be simplified as:

$$D_{Li} = \frac{4}{\pi\tau}\left(\frac{m_B V_M}{M_B A}\right)^2 \left(\frac{\Delta E_s}{\Delta E_\tau}\right)^2 \tag{3}$$

Fig. 9c shows an excellent linear relationship of E versus $\tau^{1/2}$, which indicates that Eq. (3) is suitable for the calculation of D_{Li+}. The parameters in the equation can be obtained from the GITT curves. The geometric surface area of the electrode is taken as the total contact area (A) between the electrode and the electrolyte. As the actual surface area in contact with the active material in a composite electrode will be larger than the geometric surface area due to the penetration of electrolyte into the electrode, the D_{Li+} values will accordingly have some uncertainty. So the D_{Li+} values obtained by Eq. (3) for LVO_3 compound are to be treated as the empirical (apparent) rather than the true values [51,52]. The values of D_{Li+} are in the range from 10^{-10} to 10^{-8} cm^2 s^{-1} during the charge–discharge processes as plotted in Fig. 9d. There is little difference of the D_{Li+} calculated by the different two methods, which also can be seen in other research [53]. The high D_{Li+} in the $LiVO_3$ electrode indicates a good kinetics characteristic.

4. Conclusions

Pure $LiVO_3$ compound was synthesized by combustion synthesis method with oxalic acid as fuel. This method is simple and can synthesize materials with good performance in a relatively short calcination time. The $LiVO_3$ calcined at 450 °C for 2 h displays optimal electrochemical performances, delivering a high discharge capacity of 298.4 mAh g^{-1} and 262.5 mAh g^{-1} between 1.0 and 3.5 V at a current density of 50 mA g^{-1} and 500 mA g^{-1} respectively. It also exhibits good cyclic performance and small polarization. The good performance can be owing to its relatively low crystallization, small particle size and low resistance. The chemical diffusion coefficient of Li^+ in the $LiVO_3$ electrode calculated by EIS is in the range of 10^{-9}–10^{-8} cm^2 s^{-1}, while it calculated by GITT is 10^{-10}–10^{-8} cm^2 s^{-1}, which indicates a good kinetics characteristic. As a result, the $LiVO_3$ compound is a promising cathode candidate for LIBs.

Acknowledgments

This work is supported by the National Science and Technology Support Program (2012BAK30B04) and the Key Science and Technology Innovation Team of Zhejiang Province (2010R50013).

References

[1] M.S. Whittingham, Chem. Rev. 104 (2004) 4271.
[2] L.W. Su, Y. Jing, Z. Zhou, Nanoscale 3 (2011) 3967.
[3] B.L. Ellis, K. Town, L.F. Nazar, Electrochim. Acta 84 (2012) 145.
[4] S.C. Yin, H. Grondey, P. Strobel, H. Huang, L.F. Nazar, J. Am. Chem. Soc. 125 (2003) 326.
[5] L.F. Xiao, Y.Q. Zhao, Y.Y. Yang, Y.L. Cao, X.P. Ai, H.X. Yang, Electrochim. Acta 54 (2008) 545.
[6] Y.Q. Qiao, X.L. Wang, J.P. Zhou, J. Zhang, C.D. Gu, J.P. Tu, J. Power Sources 198 (2012) 287.
[7] L.Q. Mai, X. Xu, L. Xu, C.H. Han, Y.Z. Luo, J. Mater. Res. 26 (2011) 2175.
[8] S. Huang, Y. Lu, T.Q. Wang, C.D. Gu, X.L. Wang, J.P. Tu, J. Power Sources 235 (2013) 256.
[9] J.H. Song, H.J. Park, K.J. Kim, Y.N. Jo, J.-S. Kim, Y.U. Jeong, Y.J. Kim, J. Power Sources 195 (2010) 6157.
[10] X.Y. Chen, H.L. Zhu, Y.C. Chen, Y.Y. Shang, A.Y. Cao, L.B. Hu, G.W. Rubloff, ACS Nano 6 (2012) 7948.
[11] V. Pralong, V. Gopal, V. Caignaert, V. Duffort, B. Raveau, Chem. Mater. 24 (2012) 12.
[12] Y.Q. Qiao, J.P. Tu, J.Y. Xiang, X.L. Wang, Y.J. Mai, D. Zhang, W.L. Liu, Electrochim. Acta 56 (2011) 4139.
[13] J.J. Feng, X.Z. Liu, X.M. Zhang, J.Z. Jiang, J. Zhao, M. Wang, J. Electrochem. Soc. 156 (2009) 768.
[14] S.R. Jain, K.C. Adiga, V. Pai Verneker, Combust. Flame 40 (1981) 71.
[15] J.M. Amarilla, R.M. Rojas, J.M. Rojo, J. Power Sources 196 (2011) 5951.
[16] L.A. Riley, S.V. Atta, A.S. Cavanagh, Y.F. Yan, S.M. George, P. Liu, A.C. Dillon, S.H. Lee, J. Power Sources 196 (2011) 3317.
[17] S. Patoux, M.M. Doeff, Electrochem. Commun. 6 (2004) 767.
[18] C.Z. Lu, G.T. Fey, J. Phys. Chem. Solids 67 (2006) 756.
[19] B.T. Zhao, X. Yu, R. Cai, R. Ran, H.T. Wang, Z.P. Shao, J. Mater. Chem. 22 (2012) 2900.
[20] Y.C. Si, L.F. Jiao, H.T. Yuan, H.X. Li, Y.M. Wang, J. Alloys Compd. 486 (2009) 400.
[21] Y. Sharma, N. Sharma, G.V. Subba Rao, B.V.R. Chowdari, Adv. Funct. Mater. 17 (2007) 2855.
[22] A.S. Prakash, P. Manikandan, K. Ramesha, M. Sathiya, J.-M. Tarascon, A.K. Shukla, Chem. Mater. 22 (2010) 2857.
[23] L.H. Hu, Q. Peng, Y.D. Li, J. Am. Chem. Soc. 130 (2008) 16136.
[24] D. Kovacheva, H. Gadjov, K. Petrov, S. Mandal, M.G. Lazarraga, L. Pascual, J.M. Amarilla, R.M. Rojas, P. Herrero, J.M. Rojo, J. Mater. Chem. 12 (2002) 1184.
[25] A. Subramania, N. Angayarkanni, T. Vasudevan, Mater. Chem. Phys. 102 (2007) 19.
[26] J.S. Park, K.C. Roh, J.W. Lee, K. Song, Y. Kim, Y.M. Kang, J. Power Sources 230 (2013) 138.
[27] M. Minakshi, S. Kandhasamy, D. Meyrick, J. Alloys. Compd. 544 (2012) 62.
[28] Gangulibabu, D. Bhuvaneswari, N. Kalaiselvi, J. Solid-State Electrochem. 17 (2013) 9.
[29] L. Zhang, H.F. Xiang, Z. Li, H.H. Wang, J. Power Sources 203 (2012) 121.
[30] S.J. Shi, J.P. Tu, Y.Y. Tang, Y.X. Yu, Y.Q. Zhang, X.L. Wang, C.D. Gu, J. Power Sources 228 (2013) 14.
[31] N. Yabuuchi, K. Yamamoto, K. Yoshii, I. Nakai, T. Nishizawa, A. Omaru, J. Electrochem. Soc. 160 (2013) 39.
[32] H.S. Fang, L.P. Li, G.S. Li, J. Power Sources 167 (2007) 223.
[33] T. Li, W.H. Qiu, G.H. Zhang, H.L. Zhao, J.J. Liu, J. Power Sources 174 (2007) 515.
[34] Z. Zhu, H. Yan, D. Zhang, W. Li, Q. Lu, J. Power Sources 224 (2013) 13.
[35] K. West, B. Zachau-Christiansen, S. Skaarup, Y. Saidi, J. Barker, I.I. Olsen, R. Pynenburg, R. Koksbang, J. Electrochem. Soc. 143 (1996) 820.
[36] X.H. Xiong, Z.X. Wang, H.J. Guo, X.H. Li, F.X. Wu, P. Yue, Electrochim. Acta 71 (2012) 206.
[37] B. Pei, H.X. Yao, W.X. Zhang, Z.H. Yang, J. Power Sources 220 (2012) 317.
[38] Y.Q. Qiao, J.P. Tu, Y.J. Mai, L.J. Cheng, X.L. Wang, C.D. Gu, J. Alloys Compd. 509 (2011) 7181.
[39] Y.Q. Qiao, J.P. Tu, X.L. Wang, J. Zhang, Y.X. Yu, C.D. Gu, J. Phys. Chem. C 115 (2011) 25508.
[40] J. Yan, W. Yuan, Z.Y. Tang, H. Xie, W.F. Mao, L. Ma, J. Power Sources 209 (2012) 251.
[41] C.J. Cui, G.M. Wu, J. Shen, B. Zhou, Z.H. Zhang, H.Y. Yang, S.F. She, Electrochim. Acta 55 (2010) 2536.
[42] X.P. Zhang, H.J. Guo, X.H. Li, Z.X. Wang, L. Wu, Electrochim. Acta 64 (2012) 65.
[43] J.Y. Xiang, J.P. Tu, L. Zhang, X.L. Wang, Y. Zhou, Y.Q. Qiao, Y. Lu, J. Power Sources 195 (2010) 8331.
[44] A. Sakunthala, M.V. Reddy, S. Selvasekarapandian, B.V.R. Chowdari, P. Christopher Selvin, J. Phys. Chem. C 114 (2010) 8099.
[45] C. Ho, I.D. Raistrick, R.A. Huggins, J. Electrochem. Soc. 127 (1980) 343.
[46] Q.Q. Chen, X.C. Qiao, Y.B. Wang, T.T. Zhang, C. Peng, W.M. Yin, L. Liu, J. Power Sources 201 (2012) 267.
[47] H.P. Guo, L. Liu, Q.L. Wei, H.B. Shu, X.K. Yang, Z.H. Yang, M. Zhou, J.L. Tan, Z.C. Yan, X.Y. Wang, Electrochim. Acta 94 (2013) 113.
[48] W.L. Liu, J.P. Tu, Y.Q. Qiao, J.P. Zhou, S.J. Shi, X.L. Wang, C.D. Gu, J. Power Sources 196 (2011) 7728.
[49] X.M. Jian, J.P. Tu, Y.Q. Qiao, Y. Lu, X.L. Wang, C.D. Gu, J. Power Sources 236 (2013) 33.
[50] W. Weppner, R.A. Huggins, J. Electrochem. Soc. 124 (1977) 1569.
[51] K.M. Shaju, G.V. Subba Rao, B.V.R. Chowdari, Electrochim. Acta 48 (2003) 2691.
[52] K.M. Shaju, G.V. Subba Rao, B.V.R. Chowdari, J. Mater. Chem. 13 (2003) 106.
[53] X.H. Rui, N. Ding, J. Liu, C. Li, C.H. Chen, Electrochim. Acta 55 (2010) 2384.